Journal of the Brazilian Society of Mechanical Sciences and Engineering (2023) 45:207
https://doi.org/10.1007/s40430-023-04118-9

TECHNICAL PAPER

Comparison of experiments and simulations of thermal characteristics of a bearing-rotor system

Dongju Chen[1] · Jia Li[1] · Yuhang Tang[2] · Kun Sun[1] · Ri Pan[1] · Jinwei Fan[1]

Received: 27 July 2022 / Accepted: 18 February 2023 / Published online: 16 March 2023

Abstract
The hydrostatic spindle system is the main internal heat source of the machine tool, thus it is very significant to study the thermal behaviors of the hydrostatic spindle system. The purpose of this study is to investigate the effect of viscosity-temperature effect of lubricant on the temperature fields of hydrostatic bearing oil film and spindle thermal deformation. To study the effect of temperature rise of hydrostatic bearing oil film on the hydrostatic spindle and bearing bush, empirical equations, CFD, and experimental methods are used in this paper. Firstly, the temperature rise of hydrostatic bearing is obtained by the theoretical calculation method. Secondly, based on the CFD, the temperature field of lubricating oil film is compared and analyzed with consideration of viscous temperature effect and constant value of viscosity. Based on the fluid-thermal-solid coupling method, the thermal deformation of the spindle is analyzed. Finally, the experimental platform of the hydrostatic spindle is built and the accuracy of the simulation results was verified. The study shows that when the viscosity-temperature effect is considered, the values of oil film temperature rise and spindle thermal deformation are closer to the experimental values, and the error rates of bearing temperature and spindle thermal deformation are smaller than those when the viscosity is fixed.

Keywords Viscosity-temperature effect · Hydrostatic bearing · Thermal deformation · Fluid-thermal-solid coupling

1 Introduction

The temperature rise of an ultra-precision machine tool has a great impact on machining accuracy. As the core component in a machine tool, the spindle would generate large amounts of heat when it is running at a high speed. As the demand for high-accuracy of the machine tool becomes higher and higher, thousands of scholars and engineers are dedicated to the research of thermal characteristics analysis of spindles.

The hydrostatic spindle includes bearings in radial and axial directions, oil film, and shaft, when it works, the temperature of the oil film between the bearing and shaft will increase, thermal deformation will occur [1], and this will influence the motion accuracy of the spindle. Because thermoelastic deformation processes of machine tools are so complicated, the finite element method has been used as the major method to study them [2]. Based on the finite element method, Markin et al. [3] investigated the load-carrying capacity, oil film temperature rise, and thermal deformation of the thrust bearing. Yu et al. [4] conducted a theoretical study, numerical simulation, and experimental verification of the deformation characteristics of a double rectangular cavity liquid hydrostatic thrust bearing under extreme operating conditions and found that the thermal deformation was most pronounced on the outside of the sealed oil side of the double rectangular cavity. Zhang et al. [5] established a model of multi-oil pad hydrostatic bearing considering variable viscosity and simulated the oil film pressure field of hydrostatic bearing at different speeds by CFD software and finite volume method. It was found that the viscosity has a great influence on the pressure of heavy-duty hydrostatic bearings. However, the neglection of the thermal-structure interaction of a high-speed spindle system may lead to the modeling

Technical Editor: Daniel Onofre de Almeida Cruz.

✉ Dongju Chen
djchen@bjut.edu.cn

✉ Yuhang Tang
yuhang830@sohu.com

[1] Beijing Key Laboratory of Advanced Manufacturing Technology, Faculty of Materials and Manufacturing, Beijing University of Technology, Beijing 100124, China

[2] Beijing Institute of Control Engineering, Beijing, China

error of the thermal characteristics [6]. Therefore, Holkup et al. [7] established a thermal-structure model of the electric spindle, which can predict the temperature field distribution and temperature rise of the electric spindle. Chen et al. [8] studied the effects of thermal deformation on oil film thickness, stiffness, load capacity, and machining accuracy of a hydrostatic spindle by proposing a thermomechanical error model. In surface finishing of grinding machines, accuracy is most affected by spindle stiffness. Pham et al. [9] investigated the effect of lubricant pressure and lubricant viscosity on hydrostatic spindle stiffness. The results show that the stiffness of the hydrostatic bearing was proportional to the lubricant viscosity and pump pressure. Kim et al. [10] studied the thermal deformation of grinding machines and found that the thermal deformation of the spindle depends on the temperature of the hydrostatic bearing. Su et al. [11] built a coupled heat-flow-solid integration model of the hydrostatic spindle system and simulated the heat production process and the fluid–solid coupled heat transfer process of the system. Based on the coupled thermal-structural model, Sun et al. [12] analyzed the thermal behavior of the hydrostatic spindle considering contact thermal resistance and oil film temperature rise. The results show that the thermodynamic-based structural optimization method reduces the thermal error and improves the accuracy. Yu et al. [13] studied the thermal-fluid–solid coupling deformation and frictional failure mechanism of hydrostatic bearing frictional pairs under high-speed and heavy load conditions, revealed the deformation distribution law of bearing frictional pairs and obtained the relationship between frictional pairs deformation and speed and load. Yu et al. [14] designed a new tilting oil pad hydrostatic bearing structure and investigated the effect of tilt angle on oil film stiffness. The results show that the tilted oil pad generates additional dynamic pressure, which increases the pressure and stiffness of the oil film and improves the stability and accuracy of the hydrostatic bearing. Li et al. [15] conducted a theoretical and experimental study on the temperature of high-speed heavy load tiltable tile radial bearings. The study shows that the bearing temperature increased with the increase in static load and speed.

Yan et al. [16] took into account the thermal-structural interaction and developed a network method for spindle transient analysis. Zhang et al. [17] developed an active cooling strategy for spindle thermal balance control to accurately eliminate disturbing heat transfer. To achieve model accuracy, Xiang et al. [18] proposed a new data-driven prediction (DDP) method and applied it to model the dynamic linearization of spindle thermal errors. Meng et al. [19] analyzed various fractal parameters influenced by a thermal resistance network model of the motorized spindle, and Wu et al. [20] used a deep learning method to predict the thermal error of the spindle, this learning model has good applicability to the spindle thermal error prediction and compensation. In addition to the modeling and impact study of the spindle thermal, Liu et al. [21] also compensate for the thermally induced error of the spindle based on long short-term memory neural networks.

Most of the current research has focused on the thermal analysis of hydraulic spindles, where viscosity is generally calculated as a constant value. However, during the actual operation of a hydrostatic spindle, the temperature of the lubricant gradually increases as the spindle speed increases, causing the lubricant viscosity to change, resulting in a change in the oil film carrying capacity, and thus making the thermal deformation of the shaft tile and rotor inconsistent with traditional theory. In addition to the influence of spindle speed, it is also related to the structural parameters of the spindle when it was initially designed. Therefore, it is necessary to establish the relationship between the temperature of the oil film in the bearing and the changing viscosity and the structural parameters of the spindle. The innovation of this paper is to study the viscous temperature effect and also to establish a coupled flow-thermal-solid model for a more accurate evaluation and prediction of the working performance of the hydrostatic spindle. In addition, a liquid hydrostatic spindle experimental bench was built to experimentally test the thermal deformation of the spindle rotor, and the experimental values were compared with the simulated values to verify the rationality of the simulation model and the reliability of the research results. This study will provide a reference for the in-depth study of the thermal characteristics of the hydrostatic spindle system.

2 Structure of hydrostatic bearing

According to the different structures and load-bearing methods of hydrostatic bearings, the hydrostatic bearing is divided into a radial bearing and a thrust bearing. The radial bearing bears the load in the radial direction of the spindle, and the thrust bearing bears the load in the axial direction of the spindle. In the hydrostatic spindle system, the positioning of the spindle is achieved through the cooperation of radial bearings and thrust bearings. Based on the machine tool spindle system and equipment parameters in this laboratory, the radial bearing is a four-cavity structure, the thrust bearing is a six-cavity structure, and the bearing is throttled by small holes. Figure 1 is a schematic diagram of the structure of a hydrostatic bearing, and Table 1 is a structural parameter of the hydrostatic bearing.

3 Method

3.1 Theoretical calculation of oil film temperature rise of hydrostatic bearing

1. Radial oil film temperature rise calculation

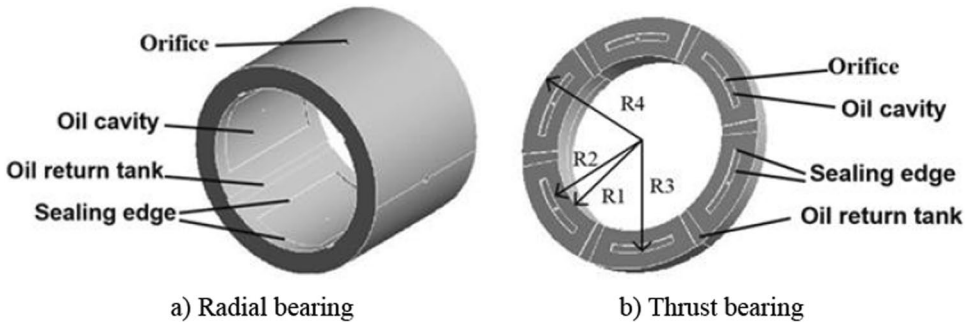

Fig. 1 Structure of hydrostatic bearing

Table 1 Structural parameters of hydrostatic bearing

Radial bearing				Thrust bearing			
Flow Coefficient	0.7	The angle of oil cavity (°)	54	Bearing inner diameter R1(mm)	35	Oil chamber angle (°)	18°
Bearing length (mm)	70	Oil cavity length (mm)	56	Seal oil edge inner diameter R2(mm)	41	Half angle of oil cushion (°)	27°
Spindle radius (mm)	35	Oil film thickness (mm)	0.01	Seal oil edge outer diameter R3(mm)	44	Lubricant density (kg/m3)	858
Oil seal edge length factor	0.8	Radial oil cavity length factor	1.6	Bearing outer diameter R4(mm)	50.5	Lubricant viscosity (Pa.s)	0.00575
Throttle diameter (mm)	0.8	Half angle of oil cushion (°)	42	Oil film thickness (mm)	0.012	Specific heat capacity of lubricant (J/kg· ℃)	2000
Supply pressure (MPa)	1.8			Orifice diameter (mm)	1.2	Thermal conductivity of lubricating oil (W/ m·℃)	0.144

The frictional power N_t of hydrostatic bearing oil film is calculated according to the Newton shear stress formula:

$$N_t = 4F_t \times u = 4\mu\left[\frac{A_1}{h_0} + \frac{A_2}{h_0 + z_1}\right]\left(\frac{\pi \mathrm{nd}}{60}\right)^2 \tag{1}$$

F_t is the shear force of the oil film, u is the linear speed of the shaft, A_1 is the seal area of the oil cavity, A_2 is the area of the oil cavity, h_0 is the oil film thickness, z_1 is the depth of radial bearing oil cavity, π is the ratio of circumference to diameter, n is the rotational speed, and d is the shaft journal.

The output power of the oil pump:

$$N_p = p_p \cdot Q_p \tag{2}$$

N_p is the output power of the oil pump, P_p is the rated oil supply pressure of the oil pump, and Q_p is the flow of the radial bearing.

The radial bearing has four oil chambers, so the flow of the radial bearing is

$$Q_p = 4Q_1 \tag{3}$$

$$Q_1 = K_0 \frac{\pi d_0^2}{4}\sqrt{\frac{2(P_s - P_{b0})}{\rho}} \tag{4}$$

$$P_s = (1 + \lambda)P_{b0} \tag{5}$$

$$\lambda = \frac{1}{2}\left(\sqrt{\frac{8\rho r^2 h_0^6 \frac{b}{w} + \theta)^2}{9\pi^2\mu^2 L^2 K_0^2 d_0^4}P_s + 1} - 1\right) \tag{6}$$

Q_p is the flow of the radial bearing, Q_1 is the flow of the individual oil chamber, K_0 is the flow coefficient, π is the ratio of circumference to diameter, d_0 is the throttle orifice diameter, P_s is the external oil supply pressure, P_{b0} is the oil cavity pressure, ρ is the density of the oil, λ is the liquid resistance ratio of the lubricating oil, b is the oil cavity length coefficient, w is the axial seal oil surface length coefficient, L is the axial seal oil surface length, u is the linear speed of the shaft, h_0 is the oil film thickness, r is the radius of the spindle, and θ is the oil cavity half angle.

The temperature rise of the radial bearing oil film is composed of the frictional power of the oil film and the power consumed by the oil pump. The temperature rise of the radial oil film is calculated as

$$\Delta t = \frac{N_t + N_p}{\rho c Q_p} \tag{7}$$

Δt is the temperature rise of the radial oil film, N_t is the frictional power of hydrostatic bearing oil film, N_p is the output power of the oil pump, ρ is the density of the oil, Q_p is the flow of the radial bearing, and c is the specific heat capacity.

2. Calculation of thrust oil film temperature rise

When calculating the temperature rise of the hydrostatic thrust bearing oil film, a simplification is performed for each oil pad of the thrust bearing model, as shown in Fig. 2, the oil sealing surface is divided into five areas and calculated separately.

Solve the oil film friction power of five divided areas:

$$N_{f1} = N_{f2} = \int_{R2}^{R3} \mu\left(\frac{2\pi Rn}{60}\right)^2 \left(\frac{(R_3 - R_2)\alpha_1 R_3}{h_0}\right) dR \tag{8}$$

$$N_{f3} = \int_{R3}^{R4} \mu\left(\frac{2\pi Rn}{60}\right)^2 \left(\frac{R(\alpha_2 + 2\alpha_1)}{h_0}\right) dR \tag{9}$$

$$N_{f4} = \int_{R2}^{R3} \mu\left(\frac{2\pi Rn}{60}\right)^2 \left(\frac{R\alpha_2}{h_0 + z}\right) dR \tag{10}$$

$$N_{f5} = \int_{R1}^{R2} \mu\left(\frac{2\pi Rn}{60}\right)^2 \left(\frac{R(\alpha_2 + 2\alpha_1)}{h_0}\right) dR \tag{11}$$

The friction power of the thrust bearing oil film is

$$N_f = 6(N_{f1} + N_{f2} + N_{f3} + N_{f4} + N_{f5}) \tag{12}$$

N_f is the friction power of the oil chamber of the thrust bearing, R_1 is the bearing inner diameter, R_2 is the seal oil edge inner diameter, R_3 is the seal oil edge outer diameter, R_4 is the bearing outer diameter, π is the ratio of circumference to diameter, u is the linear speed of the shaft, n is the rotational speed, z_1 is the depth of radial bearing oil cavity, h_0 is the oil film thickness, α_1 is the oil chamber angle, and α_2 is the half angle of oil cushion.

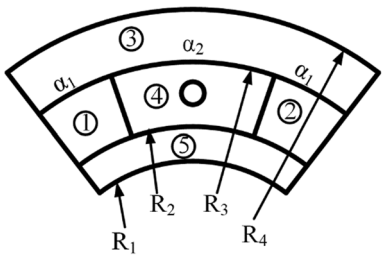

Fig. 2 Simplified model of thrust bearing seal surface

The thrust bearing oil pump power calculation is the same as the radial oil pump power calculation method.

Oil pump output power of thrust bearing:

$$N_r = p_p \cdot Q_r \tag{13}$$

The temperature rise of the thrust bearing oil film is

$$\Delta t = \frac{N_f + N_r}{\rho c Q_r} \tag{14}$$

Nr is the oil pump output power of thrust bearing, P_p is the rated oil supply pressure of the oil pump, Q_r is the flow of the thrust bearing, Δt is the temperature rise of the thrust bearing oil film, N_f is the friction power of the oil chamber of the thrust bearing, ρ is the density of the oil, and c is the specific heat capacity.

3.2 Simulation of oil film temperature field and thermal deformation of hydrostatic bearing

(1) Visco-temperature effect

The viscosity of lubricants is strongly influenced by temperature. Therefore, the viscosity-temperature relationship equation for industrial 3# white oil is fitted based on the Reynolds model ($\mu = be^{aT}$) in this paper as follows:

$$\mu = 7.045e^{-0.02441(X+T)} \tag{15}$$

μ is the dynamic viscosity value at temperature X, X is the temperature rise of lubricating oil, T is the Reference temperature, and $T = 273.15$ K.

(2) Hydrostatic bearing oil film meshing and boundary conditions

In this paper, the radial oil film and thrust oil film of the hydrostatic bearing studied are very thin with a thickness of only 10 μm, it is very difficult to divide the mesh. Thus, the following assumptions are made before dividing the mesh: (1) Ignoring the small radius rounded corners in the oil cavity of the hydrostatic bearing when building the three-dimensional model and simplifying the oil cavity to a rectangular oil cavity; (2) Assuming that throttle hole in the bearing is directly connected to the oil chamber; (3) Assuming that the 3# lubricant used is a Newtonian fluid in this paper. Figure 3 shows the simulated process of oil film temperature field and thermal deformation of the liquid hydrostatic bearing.

First, the 3D solid model of the hydrostatic bearing oil film was created in the 3D software Pro/E and exported to a ".stp" format file. Secondly, Gambit software was used to perform unstructured meshing of the oil film of the hydrostatic bearing. The mesh division results of a radial bearing and thrust bearing are shown in Fig. 3a. Thirdly, the boundary conditions of the oil film were set in Gambit software. The maximum Reynolds number of the fluid studied in this paper is 88 (< 2300), so the fluid state is set to laminar flow in the CFD package, the inlet and outlet of the bearing oil film are set to "pressure inlet" and "pressure outlet," respectively. The inner wall surface is set as a rotating wall surface and the outer wall surface is set as a fixed wall surface. The pressure–velocity coupling algorithm SIMPLE is used to solve the oil film numerically by adjusting the relaxation factor appropriately. The process of setting boundary conditions is shown in Fig. 3(b). When setting the boundary conditions of the spindle shaft, elastic constraints are set in the radial and thrust directions, respectively, to simulate the constraints of the radial and thrust bearings on the shaft. After the above work is completed, the simulation analysis of the temperature field and heat deformation can be carried out.

3.3 Liquid hydrostatic spindle flow-thermal-solid coupling analysis

The change in the viscosity of the lubricant during the operation of the hydrostatic spindle changes the temperature rise of the oil film, and the transfer of heat from the lubricant film will cause the temperature of the spindle and the bearing bush to rise and cause thermal deformation. In this paper, the coupled flow-thermal-solid analysis is carried out with the help of Workbench software. Firstly, a three-dimensional model of the spindle and the bearing bush is built, and material properties and boundary conditions are defined. Next, based on the simulation results of the fluid-hydrostatic bearing oil film, the corresponding temperature and pressure loads are applied to the coupling contact surface of the hydrostatic bearing, and the thermal-structural coupling and force-structural coupling analyses are carried out to obtain

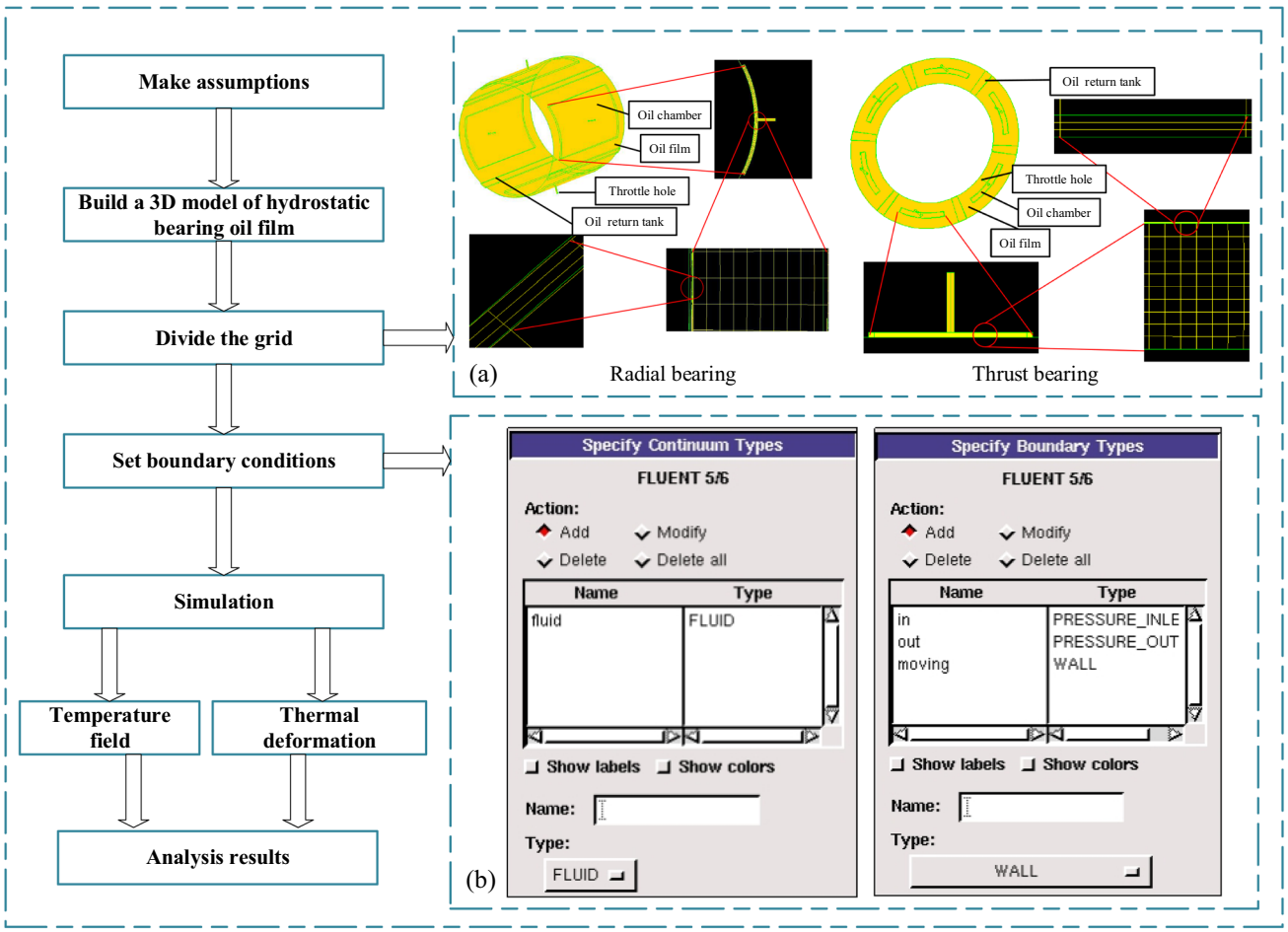

Fig. 3 Schema of the simulation

the thermal deformation of the spindle and the bearing bush, respectively.

During the numerical simulation, the speed values were selected within 0–2000 rpm. This is because the liquid hydrostatic spindle speed in the laboratory is limited between 0 and 2000 rpm. This speed interval was chosen for better comparison of simulation results with experimental results.

3.4 Experimental verification

The hydrostatic spindle experiment is conducted to verify that the above simulation is valid. The test equipment consists of a hydrostatic spindle, a fuel tank, a cooling device, a loading device, and a control cabinet, as shown in Fig. 4. The temperature of the radial bearing and thrust bearing of the hydrostatic bearing was detected by the Fluck-Ti32 thermal imager, and the thermal deformation of the spindle was tested by the SEA9 (Spindle Error Analyzer) rotation error analyzer produced by the American Lion Precision company, as shown in Fig. 5.

4 Results and discussion

4.1 Analysis of theoretical calculation and simulation results

1. Temperature

Simulate the temperature field of radial oil film and thrust oil film of hydrostatic bearing at 1000 rpm, 1200 rpm, 1500 rpm, 1800 rpm, and 2000 rpm, respectively. The cloud diagram of the temperature field of the radial oil film is shown in Fig. 6. The temperature field cloud of the thrust oil film is shown in Fig. 7.

The oil film temperature rise of the bearing at different speeds is simulated, respectively, and the oil film

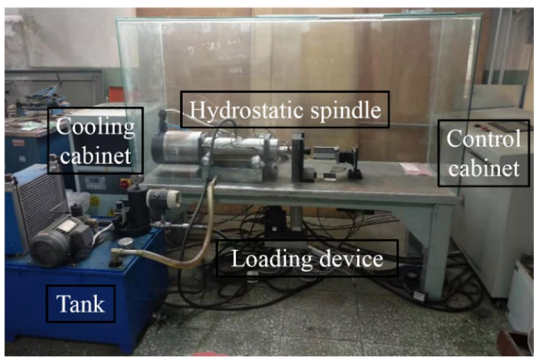

Fig. 4 Hydrostatic spindle test equipment

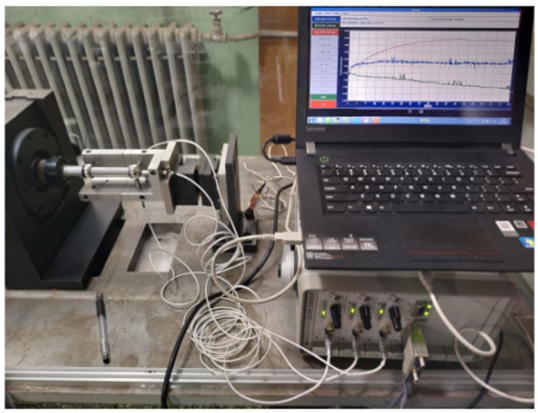

Fig. 5 Temperature measurement process

temperature rise obtained from the simulation and theoretical calculation is compared and analyzed, as shown in Fig. 8. It is found that at the same speed, the oil film temperature rise value without considering the viscosity-temperature effect is greater than the theoretical calculation value, and the theoretical calculation value is greater than when the viscosity-temperature effect is considered. The temperature rise of the oil film is found to be closer to the theoretical calculation value when considering the viscosity-temperature effect. In addition, the results of coupling with hydrostatic bearings show that the overall temperature of the bearing is lower compared to when the viscosity of the lubricant is at a constant value.

2. Bearing bush temperature

In this paper, the temperature field of the bearing bush is simulated for the liquid hydrostatic spindle speed of 1000, 1200, 1500, 1800, and 2000 prm. The effect of viscous temperature effect on the temperature field of the bearing bush is compared and analyzed. The temperature value of the bearing bush at different speeds is shown in Table 2. The results show that the viscous temperature effect has a greater impact on both radial bearing bush and thrust bearing bush, and the bearing bush temperature is lower when the viscous temperature effect is considered. As the speed increases, the viscous temperature effect is more obvious.

3. Thermal deformation

In this paper, the thermal deformation of the spindle is also simulated. The thermal deformation values of the spindle at different speeds are shown in Table 3. The thermal deformation of the spindle shaft in the axial direction is larger than the radial thermal deformation. The radial thermal deformation is almost the same in the X and Y

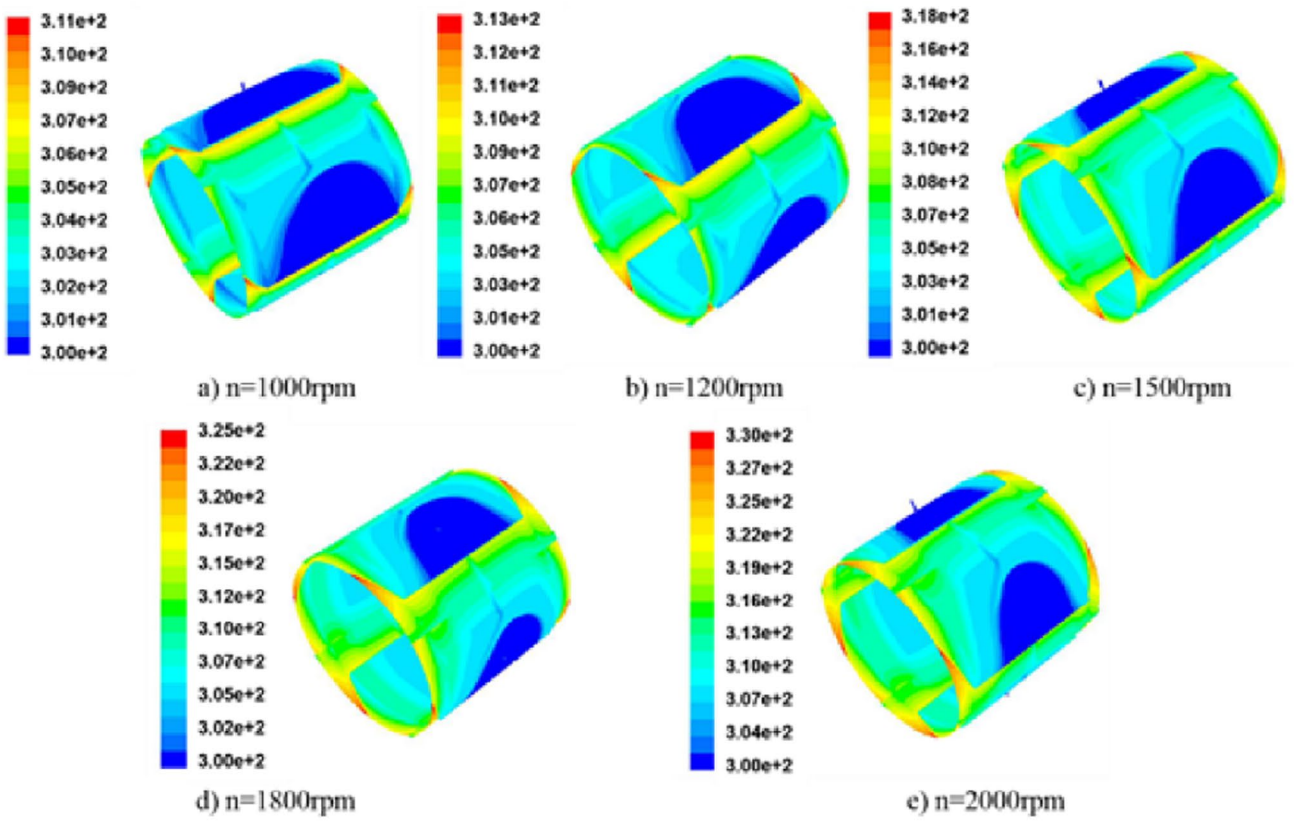

(a) Radial oil film temperature cloud at constant viscosity

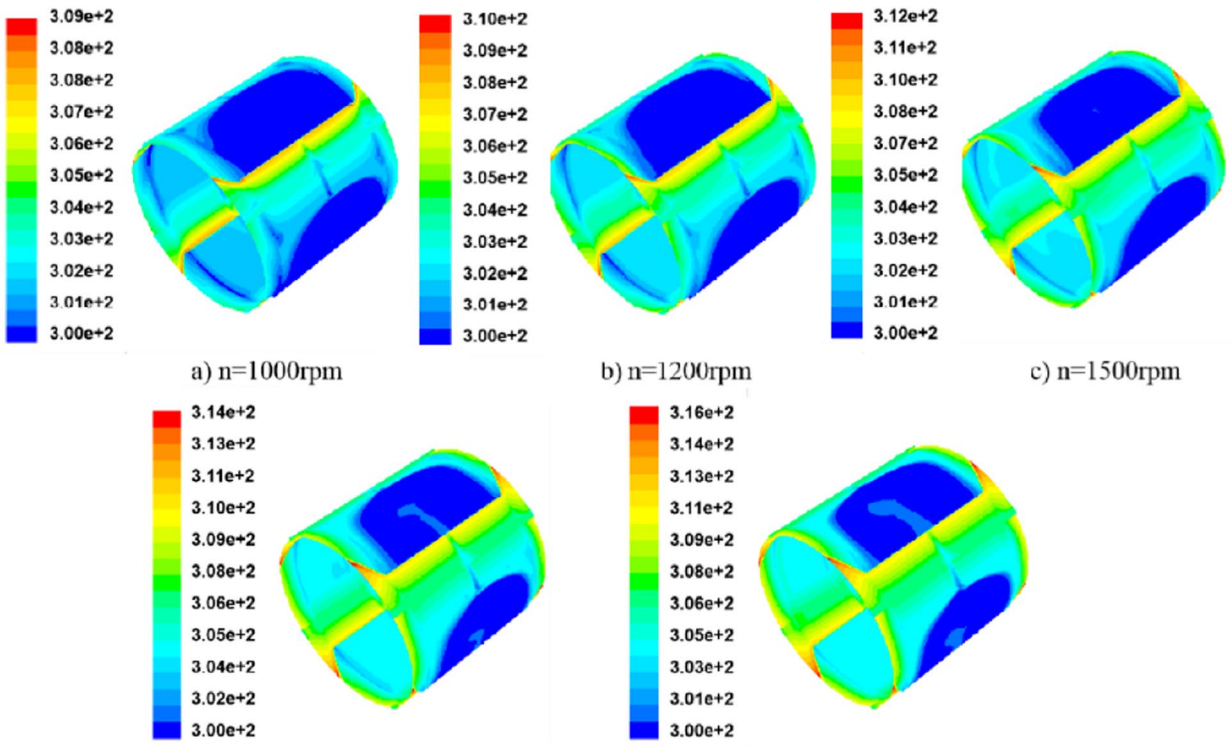

(b) Radial oil film temperature cloud diagram when viscosity changes

Fig. 6 Cloud diagram of radial oil film temperature

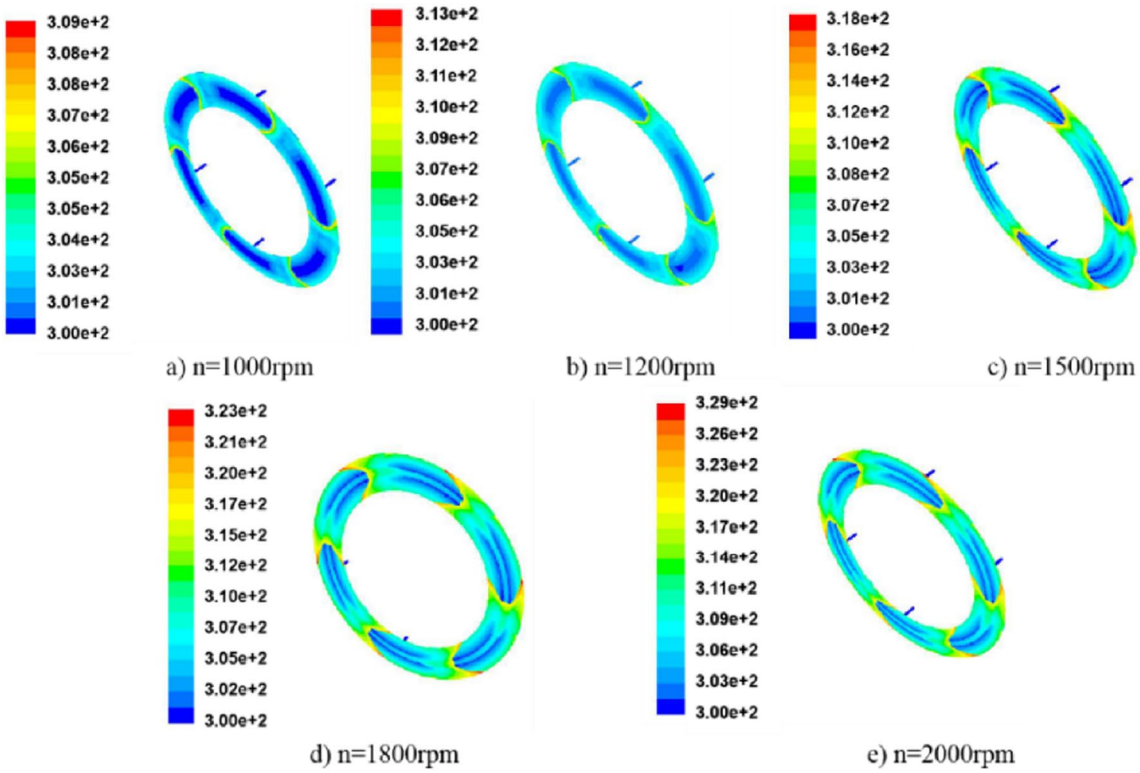

(a) Thrust oil film temperature cloud diagram at constant viscosity

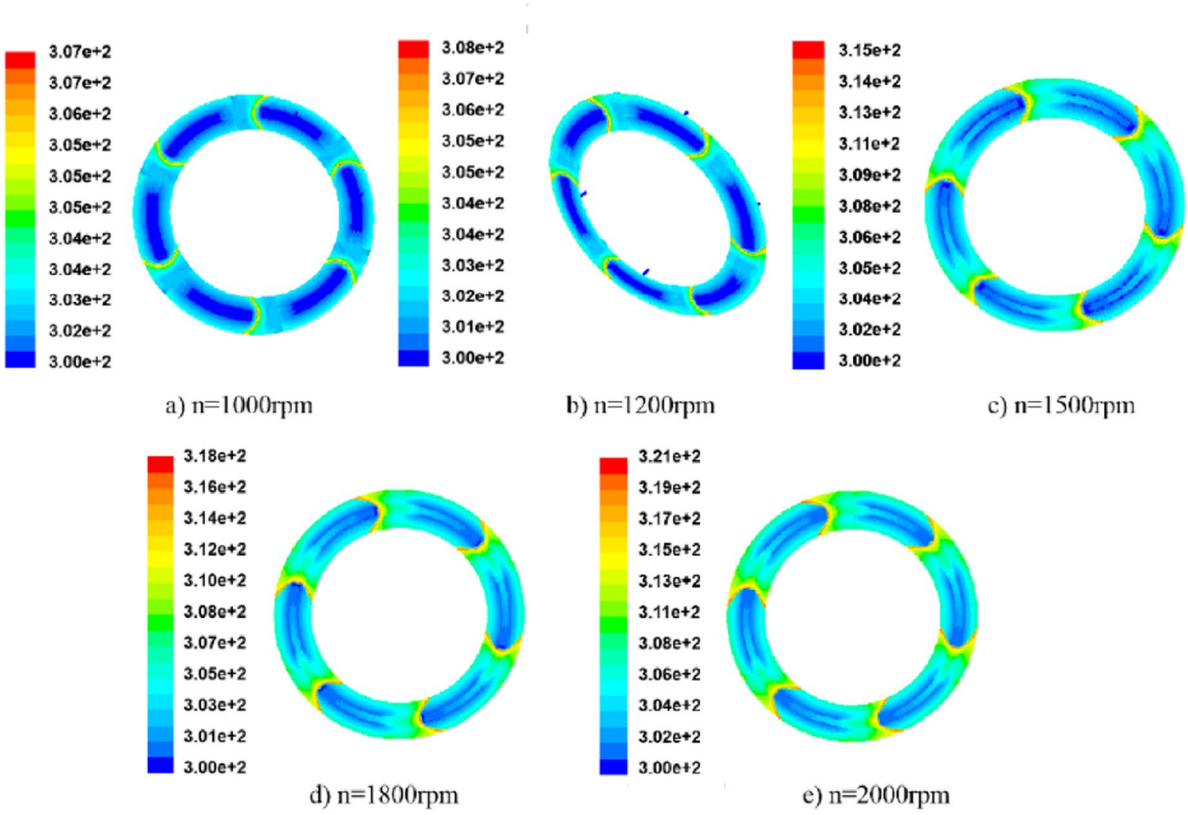

(b) Thrust oil film temperature cloud diagram when viscosity changes

Fig. 7 Cloud diagram of thrust oil film temperature

directions. When the viscosity-temperature effect is considered, the thermal deformation of the shaft in three directions is smaller than the corresponding thermal deformation value without considering the viscosity-temperature effect.

4.2 Experimental results

1. Comparative analysis of experimental and simulation results

Before measurement, the hydrostatic spindle is preheated at the start-up state. After the spindle reaches thermal equilibrium, the hydrostatic spindle speed is adjusted to 1000 rpm. The temperature of the radial and thrust bearing of the hydrostatic bearing is detected using the Fluck-Ti32 thermal imager. During the test, measure one data per minute, a total of 30 data are measured, and then use the average value as the temperature of the bearing pad. The other speed measurement methods are the same. A comparative analysis was performed between the measured temperature value of the bearing in the experiment and the simulated bearing temperature at the viscosity-temperature effect and the fixed viscosity value, and the results are shown in Fig. 9. It can be concluded from Fig. 9 that the temperature of the radial bearing and the thrust bearing increase with the increase in the rotation speed. The value of the bearing temperature at a fixed viscosity value is greater than the experimental value, and the measured value of the experiment is greater

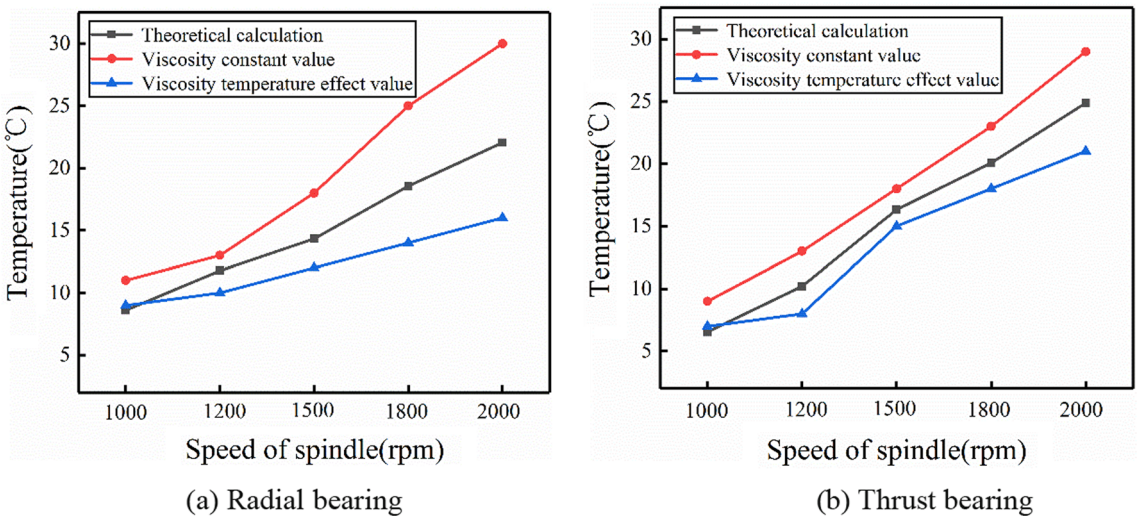

Fig. 8 Oil film temperature rise comparison

Table 2 Temperature value of bearing bush

		1000 rpm	1200 rpm	1500 rpm	1800 rpm	2000 rpm
Viscosity constant	Radial bearing bush temperature (℃)	36.58	40.40	45.19	51.15	55.95
	Thrust bearing bush temperature (℃)	34.25	36.22	44.27	48.90	51.67
Viscosity change	Radial bearing bush temperature (℃)	34.54	37.11	36.65	40.52	42.52
	Thrust bearing bush temperature (℃)	32.05	33.41	38.93	41.95	43.88

Table 3 Thermal deformation value of spindle

		1000 rpm	1200 rpm	1500 rpm	1800 rpm	2000 rpm
Viscosity constant	X–thermal deformation (μm)	4.47	4.98	7.45	10.55	14.32
	Y–thermal deformation (μm)	4.46	5.16	7.46	10.56	14.28
	Z–thermal deformation (μm)	12.51	14.30	19.96	25.56	28.50
Viscosity change	X–thermal deformation (μm)	4.03	4.10	5.84	6.98	8.68
	Y–thermal deformation (μm)	4.03	4.16	5.56	6.96	8.64
	Z–thermal deformation (μm)	11.33	11.93	15.93	18.57	20.89

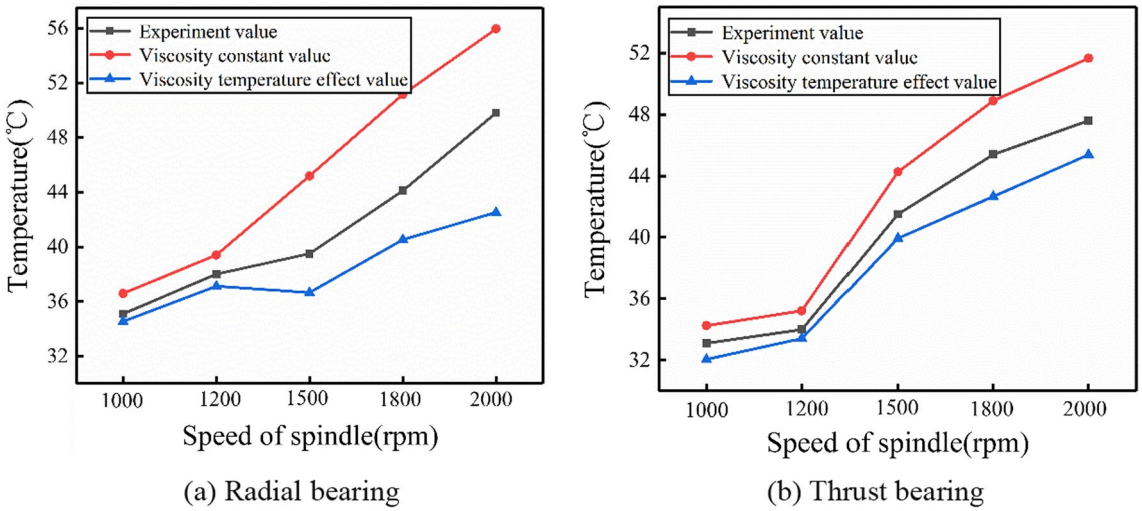

Fig. 9 Bearing temperature of hydrostatic bearing

than the value of the bearing temperature at the viscosity-temperature effect.

Based on the hydrostatic spindle testbed, a SEA9 (Spindle Error Analyzer) rotary error analyzer produced by the American Lion Precision company was used to test the thermal deformation of the spindle shaft in the *x*, *y*, and *z* directions at 1000, 1200, 1500, 1800, and 2000 rpm. After 30 min of test time, it tends to be in a state of thermal equilibrium. The maximum value is taken as the deformation result and compared with the simulated viscosity constant and the thermal deformation value of the shaft under the effect of viscosity-temperature. The thermal deformation of the shaft is shown in Fig. 10. It can be concluded that with the increase in the rotation speed, the thermal deformation of the spindle shaft in the three directions of *X*, *Y*, and *Z* increases continuously. The thermal deformation values in the *X* and *Y* directions are the same. Thermal deformation measured experimentally is smaller than the simulated value when the specific viscosity is a fixed value and is larger than when the viscosity-temperature effect is considered.

2. error analysis of the simulation

Based on the fluid-thermal-solid coupling, the temperature field of the hydrostatic bearing and the thermal deformation result of the shaft are obtained. The experimental value is compared with the results of the viscosity-temperature effect and the viscosity constant value. The analysis of the bearing temperature error rate is shown in Fig. 11. The thermal distortion error rate analysis of the shaft in three directions is shown in Fig. 12.

It can be concluded from Fig. 11 that the temperature error of radial bearing and thrust bearing increases with the increase in speed, and the error also becomes larger. When considering the viscosity-temperature effect, the temperature error of the radial bearing and thrust bearing is smaller than the error value when the viscosity is fixed. The temperature error rate of the bearing bush is the largest at 2000 rpm, and the temperature error rates of the radial bearing and thrust bearing are 11.05 and 7.82% when the viscosity-temperature effect is considered. The temperature error rates of the radial bearing and thrust bearing are 17.05 and 8.55% when the viscosity-temperature effect is without consideration.

It can be concluded from Fig. 12 that with the increase in the rotation speed, the temperature error of the spindle in the three directions of *X*, *Y*, and *Z* continuously increases, reaching a maximum of 2000 rpm. When considering the viscosity-temperature effect, the maximum thermal deformation error rates of the shaft in the three directions of *X*, *Y*, and *Z* are 18.57, 18.10, and 12.03. When the viscosity is fixed, the maximum thermal deformation error rates of the shaft in the three directions of *X*, *Y*, and *Z* are 34.33, 35.36, and 24.4%.

During the actual operation of the bearings, the temperature rise generated by internal friction of the lubricant between the bearing gaps reduces the viscosity of the lubricant. Compared to a constant viscosity, a lubricant with a dynamic change in viscosity creates a lower temperature field (lower viscosity, faster flow of lubricant between the bearings, and therefore faster heat dissipation), resulting in less thermal deformation of the spindle rotor. In addition, the numerical simulations are under ideal conditions and do not take into account the effects of factors such as ambient temperature and cooling system during the actual experiments; therefore, the simulated values are slightly smaller than the experimental values.

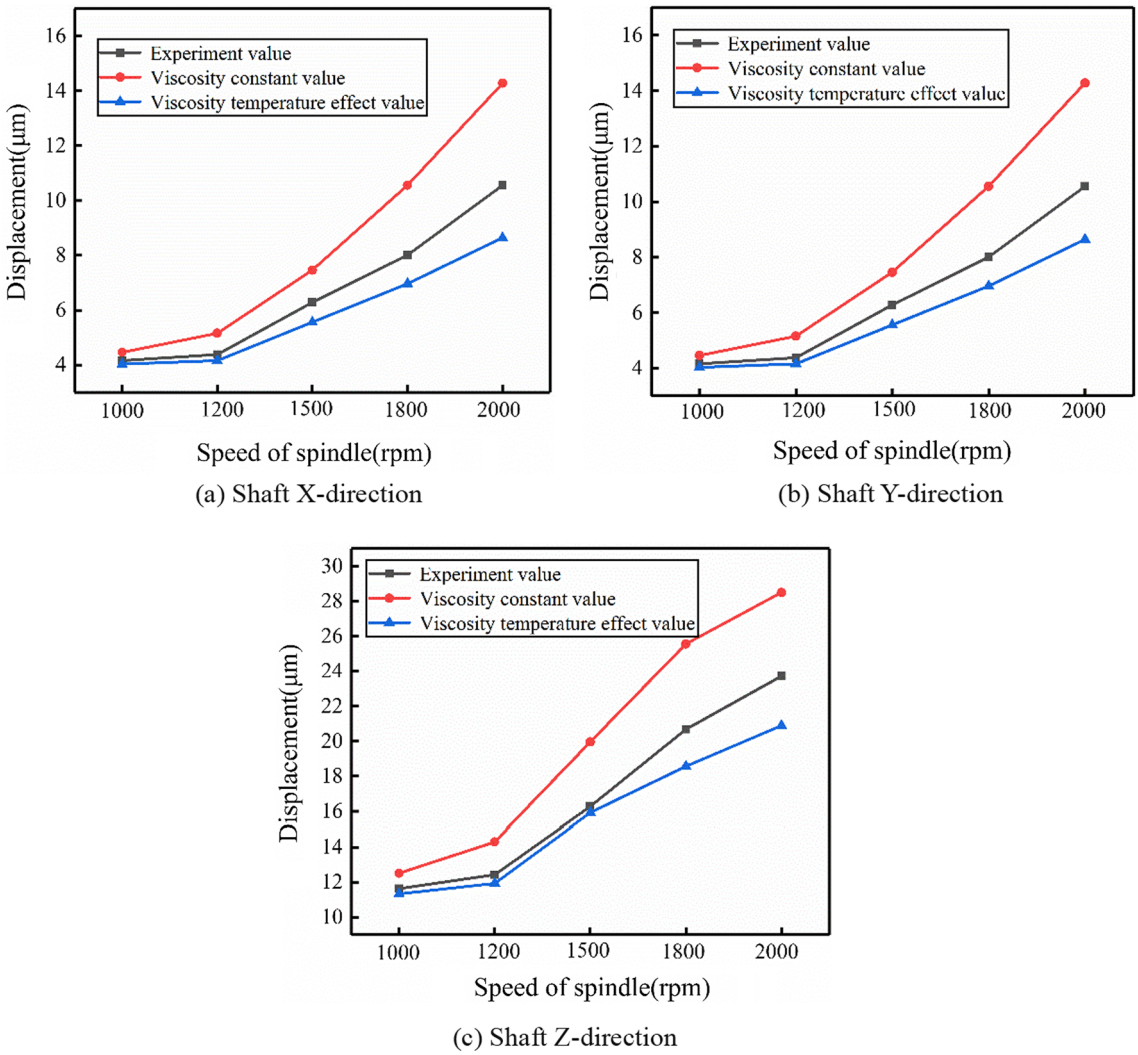

Fig. 10 Thermal deformation of the hydrostatic spindle shaft

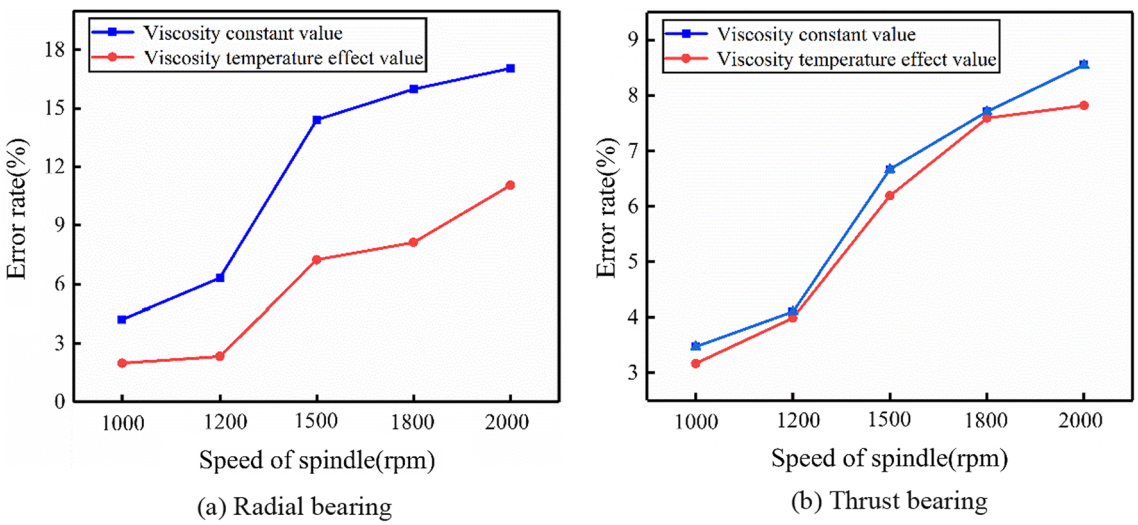

Fig. 11 Temperature error analysis of hydrostatic bearing

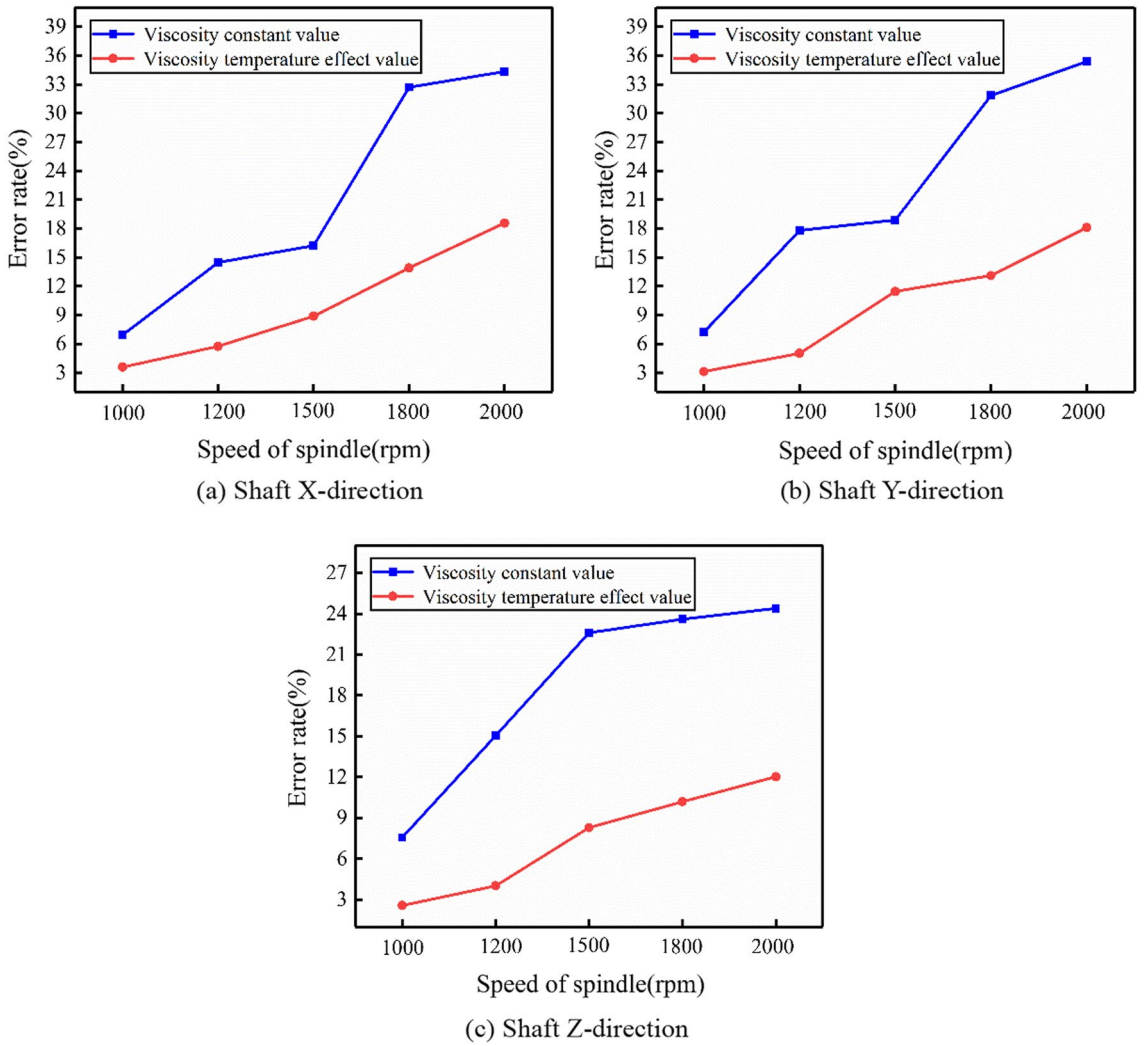

Fig. 12 Error analysis of temperature difference of spindle deformation

5 Conclusion

In this paper, the viscous temperature effect was studied, and a fluid-thermal-solid coupling model was established to evaluate and predict the working performance of the hydrostatic spindle more accurately. In addition, a liquid hydrostatic spindle experimental bench is built and the experimental values are compared with the simulated values to verify the rationality of the simulation model and the reliability of the research results. This study will provide a reference for an in-depth study of the thermal characteristics of hydrostatic spindle systems. The specific results of the study are as follows.

1. Both theoretical calculations and simulation analysis were used to analyze the oil film temperature rise. The results show that the main factor influencing the temperature rise of the hydrostatic bearing oil film is the rotational speed. With the increase in speed, the viscosity-temperature effect becomes more obvious. The oil film temperature rises when the viscosity-temperature effect considered is closer to the theoretical calculation value.
2. Considering the viscosity-temperature effect and the constant viscosity value, it is found that the thermal deformation of the spindle in the axial direction is more obvious than in the radial direction.
3. The larger the speed, the greater the error rate of the temperature of the bearing bush and the thermal deformation of the spindle. When considering the viscosity-temperature effect, the error rate of the bearing temperature and the thermal deformation of the shaft are smaller than the error rate when the viscosity is fixed.
4. Based on the liquid hydrostatic spindle experimental platform, the bearing temperature rise and thermal

deformation were tested to verify the reliability of the simulation data.

Author contributions All authors contributed to the study conception and design. Material preparation, data collection and analysis were performed by DC and JL. The first draft of the manuscript was written by JL and all authors (DC, JL, YT, KS, RP, and JF) commented on previous versions of the manuscript. All authors read and approved the final manuscript.

Funding This research was funded by the National Natural Science Foundation of China Grant No. (51875005 and 51475010).

Data availability Data in the paper are not related to other published datasets. This paper lists some relevant data of the method in the figures and tables, and other data are available from the corresponding author upon request.

Declarations

Conflict of interest The authors have no relevant financial or non-financial interests to disclose.

References

1. Ibaraki S, Inui H, Hong C, Nishikawa S, Shimoike M (2019) On-machine identification of rotary axis location errors under thermal influence by spindle rotation. Precis Eng J Int Soc Precis Eng Nanotechnol 55:42–47. https://doi.org/10.1016/j.precisioneng.2018.08.005
2. Kim JJ, Jeong YH, Cho DW (2004) Thermal behavior of a machine tool equipped with linear motors. Int J Mach Tools Manuf 44(7–8):749–758. https://doi.org/10.1016/j.ijmachtools.2004.02.006
3. Markin D, McCarthy DMC, Glavatskih SB (2003) A FEM approach to simulation of tilting-pad thrust bearing assemblies. Tribol Int 36(11):807–814. https://doi.org/10.1016/s0301-679x(03)00097-5
4. Yu X, Wang F, Zhou D, Huang D, Zhan S, Yu M, Jiao J, Wang J (2020) Deformation characteristics of adaptive hydrostatic thrust bearing under extreme working conditions. J Braz Soc Mech Sci Eng. https://doi.org/10.1007/s40430-020-02571-4
5. Zhang YQ, Fan LG, Li R, Dai CX, Yu XD (2013) Simulation and experimental analysis of supporting characteristics of multiple oil pad hydrostatic bearing disk. J Hydrodyn 25(2):236–241. https://doi.org/10.1016/s1001-6058(13)60358-3
6. Liu JL, Ma C, Wang SL, Wang SB, Yang B, Shi H (2019) Thermal-structure interaction characteristics of a high-speed spindle-bearing system. Int J Mach Tools Manuf 137:42–57. https://doi.org/10.1016/j.ijmachtools.2018.10.004
7. Holkup T, Cao H, Kolar P, Altintas Y, Zeleny J (2010) Thermo-mechanical model of spindles. Cirp Annals Manuf Technol 59(1):365–368. https://doi.org/10.1016/j.cirp.2010.03.021
8. Chen DJ, Bonis M, Zhang FH, Dong S (2011) Thermal error of a hydrostatic spindle. Precis Eng J Int Soc Precis Eng Nanotechnol 35(3):512–520. https://doi.org/10.1016/j.precisioneng.2011.02.005
9. Van-Hung P, Manh-Toan N, Tuan-Anh B (2020) Oil pressure and viscosity influence on stiffness of the hydrostatic spindle bearing of a medium-sized circular grinding machine. Int J Mod Phys B 34:22–24. https://doi.org/10.1142/s0217979220401566
10. Kim B-S, Bael G-T, Kim G-N, Moon H-M, Noh J-P, Huh S-C (2015) A study on the thermal characteristics of the grinding machine applied hydrostatic bearing. Trans Can Soc Mech Eng 39(3):717–728. https://doi.org/10.1139/tcsme-2015-0057
11. Su H, Lu LH, Liang YC, Zhang Q, Sun YZ (2014) Thermal analysis of the hydrostatic spindle system by the finite volume element method. Int J Adv Manuf Technol 71(9–12):1949–1959. https://doi.org/10.1007/s00170-014-5627-8
12. Sun LJ, Ren MJ, Hong HB, Yin YH (2017) Thermal error reduction based on thermodynamics structure optimization method for an ultra-precision machine tool. Int J Adv Manuf Technol 88(5–8):1267–1277. https://doi.org/10.1007/s00170-016-8868-x
13. Yu M, Yu X, Zheng X, Jiang H (2019) Thermal-fluid-solid coupling deformation of hydrostatic thrust bearing friction pairs. Ind Lubr Tribol 71(3):467–473. https://doi.org/10.1108/ilt-07-2018-0262
14. Yu X, Wu G, Zhou W, Bi H, Wang Y, Gao W, Wang J, Jiao J, Jiang H (2021) Inclination angle effect of tribological performance for hydrostatic bearing having tilting oil pad under variable viscosity conditions. J Braz Soc Mech Sci Eng. https://doi.org/10.1007/s40430-021-02946-1
15. Li PJ, Zhu YS, Zhang YY, Yue PF (2015) The investigation of the temperature of high speed and heavy haul tilting pad journal bearing. Ind Lubr Tribol 67(4):301–307. https://doi.org/10.1108/ilt-07-2013-0081
16. Yan K, Hong J, Zhang JH, Mi W, Wu WW (2016) Thermal-deformation coupling in thermal network for transient analysis of spindle-bearing system. Int J Therm Sci 104:1–12. https://doi.org/10.1016/j.ijthermalsci.2015.12.007
17. Zhang YF, Liu T, Gao WG, Tian YL, Qi XY, Wang P, Zhang DW (2018) Active coolant strategy for thermal balance control of motorized spindle unit. Appl Therm Eng 134:460–468. https://doi.org/10.1016/j.applthermaleng.2018.02.016
18. Xiang ST, Yao XD, Du ZC, Yang JG (2018) Dynamic linearization modeling approach for spindle thermal errors of machine tools. Mechatronics 53:215–228. https://doi.org/10.1016/j.mechatronics.2018.06.018
19. Meng QY, Yan XX, Sun CC, Liu Y (2020) Research on thermal resistance network modeling of motorized spindle based on the influence of various fractal parameters. Int Commun Heat Mass Transf. https://doi.org/10.1016/j.icheatmasstransfer.2020.104806
20. Wu CY, Xiang ST, Xiang WS (2021) Spindle thermal error prediction approach based on thermal infrared images: a deep learning method. J Manuf Syst 59:67–80. https://doi.org/10.1016/j.jmsy.2021.01.013
21. Liu JL, Ma C, Gui HQ, Wang SL (2021) Thermally-induced error compensation of spindle system based on long short term memory neural networks. Appl Soft Comput. https://doi.org/10.1016/j.asoc.2021.107094